

Satellite remote sensing and GIS-based multi-criteria analysis for flood hazard mapping

Francesca Franci¹ · Gabriele Bitelli¹ · Emanuele Mandanici¹ ·
Diofantos Hadjimitsis² · Athos Agapiou²

Received: 1 December 2015 / Accepted: 28 July 2016 / Published online: 11 August 2016
© Springer Science+Business Media Dordrecht 2016

Abstract This work focuses on the exploitation of very high-resolution (VHR) satellite imagery coupled with multi-criteria analysis (MCA) to produce flood hazard maps. The methodology was tested over a portion of the Yialias river watershed basin (Nicosia, Cyprus). The MCA methodology was performed selecting five flood-conditioning factors: slope, distance to channels, drainage texture, geology and land cover. Among MCA methods, the analytic hierarchy process technique was chosen to derive the weight of each criterion in the computation of the flood hazard index (FHI). The required information layers were obtained by processing a VHR GeoEye-1 image and a digital elevation model. The satellite image was classified using an object-based technique to extract land use/cover data, while GIS geoprocessing of the DEM provided slope, stream network and drainage texture data. Using the FHI, the study area was finally classified into seven hazard categories ranging from very low to very high in order to generate an easily readable map. The hazard seems to be severe, in particular, in some urban areas, where extensive anthropogenic interventions can be observed. This work confirms the benefits of using remote

✉ Francesca Franci
francesca.franci2@unibo.it

Gabriele Bitelli
gabriele.bitelli@unibo.it

Emanuele Mandanici
emanuele.mandanici@unibo.it

Diofantos Hadjimitsis
d.hadjimitsis@cut.ac.cy

Athos Agapiou
athos.agapiou@cut.ac.cy

¹ Department of Civil, Chemical, Environmental and Materials Engineering (DICAM), University of Bologna, V.le Risorgimento 2, 40136 Bologna, Italy

² Laboratory of Remote Sensing and Geoinformatics, Department of Civil Engineering and Geomatics, Cyprus University of Technology, Saripolou 2-8, 3603 Limassol, Cyprus

sensing data coupled with MCA approach to provide fast and cost-effective information concerning the hazard assessment, especially when reliable data are not available.

Keywords Flood hazard · GeoEye-1 · Object-based classification · Analytic hierarchy process · Yialias river

1 Introduction

During the past 30 years, the world has suffered from severe floods, causing hundreds of thousands of deaths, destruction of infrastructures, disruption of economic activities and losses of property for worth billions of dollars. Worldwide statistics show that flooding events are increasing as the number of people killed and the associated socioeconomic losses (Munich 2014). This is mainly due to the increased exposure of the world population to natural disaster. The world population has doubled in size from the 1960s to 2000, and areas susceptible to natural hazards have become settled (Garschagen et al. 2014).

To effectively reduce the impacts of natural disasters, a comprehensive strategy for risk management is required. The risk is the probability of harmful consequences or expected losses, resulting from interactions between hazards and vulnerable conditions (United Nations Inter-Agency Secretariat of the International Strategy for Disaster Reduction UN/ISDR 2004). Three components determine the risk (Kron 2005): the likelihood that a natural event may occur (hazard), the presence of people/property (values at risk) and their vulnerability (lack of resistance to damaging/destructive forces).

For flood risk reduction purpose, flood hazard maps are useful tools to identify flood-susceptible areas (Rahmati et al. 2015), whereas flood risk maps, produced considering the threat of flooding and its impacts (Altan et al. 2013), can be used for supporting decision-makers and emergency response units in the development of mitigation and preparedness strategies (Büchle et al. 2006; Ouma and Tateishi 2014). Different approaches have been used to provide information for flood risk management, involving different sources, such as hydraulic data, topographic maps, terrain models, land use/cover maps, inundation maps and population density. The methodologies for conducting risk assessments can be broadly classified into quantitative and qualitative (Wang et al. 2011). Quantitative approaches aim at expressing the flood hazard in terms of exceedance probabilities or expected losses, using numerical modelling. Qualitative methods, typically, rely on experts' interpretations and consider a number of factors that have an influence on the flood risk. They are mostly used for the construction of indexes by combining various indicators (Dewan 2013). Some qualitative approaches, however, incorporate the idea of ranking and weighting and may be considered semi-quantitative (Wang et al. 2011).

Quantitative methods are able to provide superior results, but they often require more data and detailed morphological information together with advanced numerical models. Qualitative and/or semi-quantitative approaches are relatively simpler to implement within a GIS and more flexible for handling heterogeneous data depending on their availability (Cervi 2009; Siddayao et al. 2014). Semi-quantitative methods proved to be useful for regional studies and for the initial screening process to provide hazards information (Sinha et al. 2008; Pradhan 2010; Krishnamurthy and Jayaprakash 2013; Van Westen 2013).

Among semi-quantitative approaches, various multi-criteria analysis (MCA) techniques have been used for flood susceptibility and vulnerability analysis and risk mapping

(Yahaya et al. 2010; Kandilioti and Makropoulos 2011; Musungu et al. 2012). MCA is a decision-making tool used for the analysis of environmental systems to evaluate a problem by giving an order of preference to multiple alternatives, on the basis of several criteria that may have different units (Carver 1991). In other words, its purpose is to compare and rank alternative options and to evaluate their consequences, according to the criteria established (Malczewski 2006). In this context, GIS systems, with their ability to handle heterogeneous spatial data, are a suitable tool for incorporating all the factors to be analysed (Chen et al. 2014). The analytic hierarchy process (AHP) is one of the widely used multi-criteria decision-making tools, because of its simplicity in implementation and interpretation, its capability in handling also poor quality data and efficiency in regional studies (Wang et al. 2011; Chen et al. 2014). Introduced and developed by Saaty (1980), the AHP procedure implements a pairwise comparison technique for deriving the priorities of the criteria in terms of their importance in achieving the goal. The decision-making process starts with dividing the problem into issues, which may optionally be divided further to form a hierarchy of issues. The pairwise comparison matrix is used for comparing the alternatives and defining the importance of each one relative to the others. Because the user gives judgments subjectively, the logical consistency of these evaluations is tested in the last stage. The ultimate outcome of the AHP is a relative score for each decision alternative, which can be used in the subsequent decision-making process (Lawal and Matori 2012; Siddayao et al. 2014; Ouma and Tateishi 2014).

In this context, satellite remote sensing can provide valuable information helping to understand spatial phenomena and supporting the decision-makers and responders in the field during disaster management activities (Gusella et al. 2007; Van Westen 2013; Boccardo 2013). In the post-event phases, satellite images provide the instantaneous and synoptic view necessary to accurately map the extent of floods (Dewan 2013). Both multi-spectral and radar data have been widely used to identify the inundated areas (Brivio et al. 2002; Gianinetto et al. 2006; Franci et al. 2015).

During the mitigation and preparedness stages, remote sensing data are usually employed for mapping landscape features (i.e. land use/land cover) and for supporting the development of risk maps. High spatial resolution images can allow for the identification of infrastructure and buildings in risk areas, for the vulnerability assessment and evaluation of the potential losses. Therefore, the integration of satellite remote sensing data with the above-described approaches can be systematically used so as to monitor areas and to prevent further destructions.

In this work, the integration of different geospatial data by means of a MCA approach is proposed, in order to develop an easily readable and rapidly accessible flood hazard map. Differently from previous works, remote sensing data are used to obtain information for pre-event risk management phases. A GIS-based AHP technique was performed to compute a composite hazard index considering morphologic and topographic flood-conditioning factors. A portion of the Yialias river watershed basin, in Nicosia district (Cyprus), was chosen as case study.

2 Study area

Located in the central part of the Cyprus island, 20 km towards the South of the capital Nicosia, the study area is about 70 km² in size, between longitudes 33°16'37" and 33°26'47" and latitudes 34°56'18" and 35°2'51" (Fig. 1). This area is the portion of the

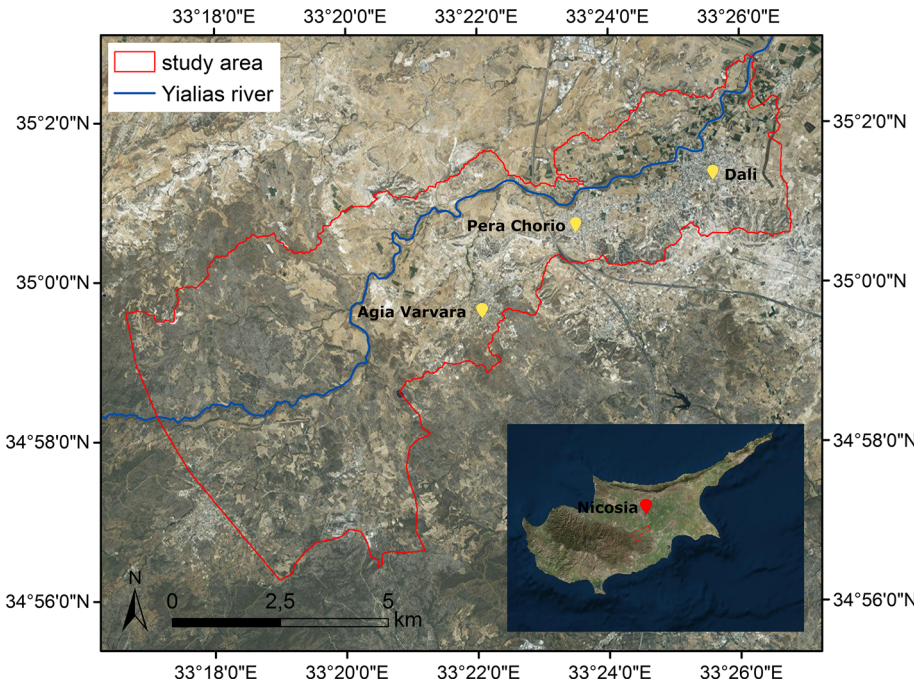


Fig. 1 Location of the study area

Yialias river watershed basin including Agia Varvara, Pera Chorio and Dali villages. The elevation ranges from 193 to 482 m a.s.l. with steep and smooth zones in the upstream and downstream areas, respectively. From west to east, metamorphic and volcanic rocks outcrop, followed by sedimentary units such as marl-chalk and alluvium/colluviums deposits.

As the most of the island rivers, the Yialias has an intermittent stream being dry during the summer season. During the last 20 years, three extreme floods occurred in this area, especially in the downstream part. According to historical data, these events took place on December 1992, February 2003 and October 2009 causing significant damages to properties and constructions (Alexakis et al. 2012, 2013). The study area is included in one of the 19 “Areas with Potential Significant Flood Risk”, identified by the Water Development Department (WDD) of the Ministry of Agriculture, Natural Resources and Environment (Republic of Cyprus, Nicosia).

3 Materials and methods

In order to produce an easily readable and rapidly accessible flood hazard map of the study area, the MCA methodology was adopted considering some parameters that control water routing when high peak flows exceed the drainage system capacity (Fernández and Lutz 2010).

Five flood-conditioning factors were selected: slope, distance to channels, drainage texture, geology and land cover, referring to previous research works and also considering the available data (Siddayao et al. 2014). In particular, the DEM of the study area was used to obtain slope, stream network, distance to main channels and drainage texture data. The

geology map was obtained converting polygon features to raster. The land cover map was produced by processing a very high-resolution satellite image (Fig. 2).

3.1 Data collection

A stereo-pair of very high-resolution GeoEye-1 images (0.5 m resolution for panchromatic and 1.65 m for multi-spectral bands), acquired on 11 December 2011 (GeoStereo™ product), was processed for land use/cover mapping to extract a 5-m pixel resolution DEM of the study area. Moreover, a 1:250.000 geological map, provided by the Cyprus Geological Survey Department, was used.

3.2 Image processing: object-based classification

Before the classification, the GeoEye-1 was subjected to radiometric calibration (TOA reflectance) and the four multi-spectral bands were orthorectified using the provided RPC model and the 5-m pixel size DEM of the study area; as the orthorectification process requires information about the height above the reference ellipsoid, a geoidal undulation equal to 28 m was considered, based on the EGM2008 gravity model (Pavlis et al. 2012). The orthorectified image was then resampled to 2 m by a bilinear interpolation. To produce the land use/cover map of the study area, the satellite image was processed using a semi-automated multi-level object-based classification, performed with eCognition 9 software (Fig. 3). The classification was performed choosing several spectral and geometric rules defined by image analysis, without using training samples.

The object-based approach is an evolving technology where textural and contextual/relational information is used in addition to spectral information for processing geospatial data (Bitelli et al. 2004; Franci et al. 2014). This procedure is particularly useful for extracting and mapping features from high spatial but low spectral resolution images (Bhaskaran et al. 2010). The classification is performed on pixel sets (image objects) derived by using image segmentation algorithms (Schiewe 2002). Segmentation phase can be carried out in a hierarchical approach, with semantic relationships between objects at different levels, allowing for effective multi-spatial resolution analysis (Taubenböck et al. 2010).

The multi-resolution segmentation algorithm, a region growing technique, was used to generate the image objects (Baatz and Schäpe 2000). Both spectral and shape heterogeneity were taken into account through user-defined colour and shape parameters. Moreover, specific scale values were set to define the acceptable level of heterogeneity: a

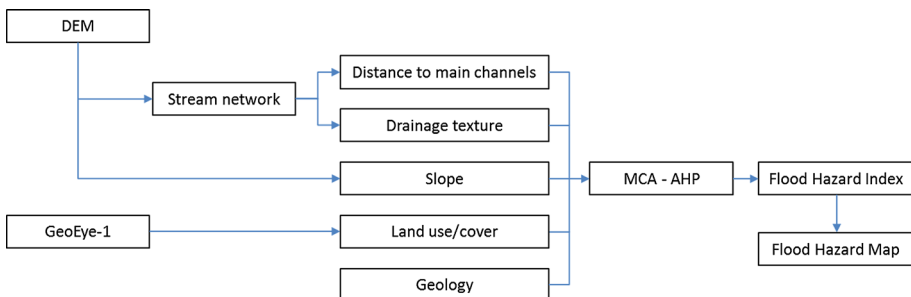


Fig. 2 Methodology workflow

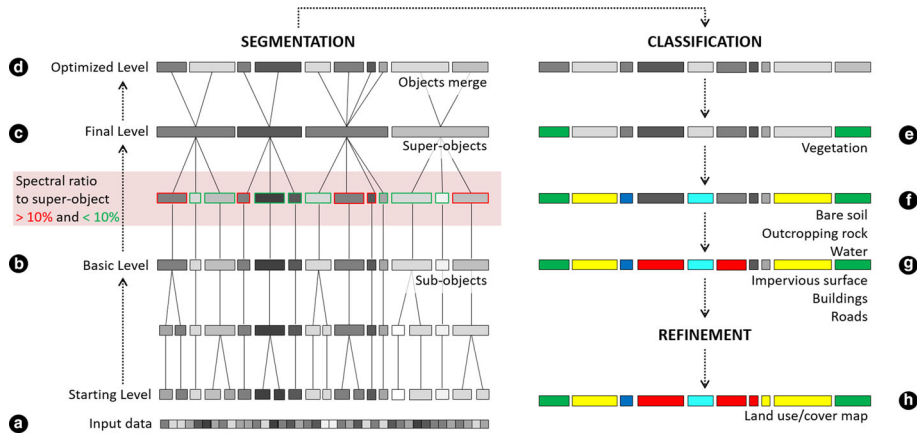


Fig. 3 Object-based procedure workflow comprising the multi-level segmentation and the classification phases *Source:* modified at Taubenböck et al. 2010

larger-scale parameter corresponds in larger objects than setting small-scale values (Benz et al. 2004).

Depending on a specific application, this method could not yield a perfect partition of the scene producing either too many and small regions (over-segmentation) or too few and large segments (under-segmentation) (Schiewe 2002). Therefore, it could be difficult to obtain objects closer to the real-world structures in a single segmentation phase. In order to overcome this limitation, a multi-level segmentation procedure was performed (Bruzzone and Carlin 2006). Each superior level was then produced by using a higher-scale parameter (Table 1). The main aim was the generation of two segmentation levels, the basic level (b in Figs. 3, 4), with a low scale value which includes small image objects in order to represent structures such as roofs, trees and streets, and the final level (c in Figs. 3, 4), with a significantly increased scale parameter, where bigger image objects represent extent areas, e.g. cultivated fields land, bare soil areas and outcrops. By means of the spectral difference between these main levels, the optimized level (d in Figs. 3, 4) was generated. In particular, whenever a sub-object in the basic level shows a significant spectral difference, “Brightness” higher than 10 %, to its super-object on the final level, the corresponding segment is reduced at the final level to its original spatial configuration. Sub-

Table 1 Segmentation parameters set for the GeoEye-1 image analysis

Level name	Scale	Homogeneity criterion		Shape settings	
		Colour	Shape	Smoothness	Compactness
Level 1	5	0.5	0.5	0.9	0.1
Level 2	15	0.5	0.5	0.9	0.1
Basic level	25	0.2	0.8	0.5	0.5
Level 3	35	0.2	0.8	0.5	0.5
Level 4	70	0.2	0.8	0.5	0.5
Final level	100	0.2	0.8	0.5	0.5

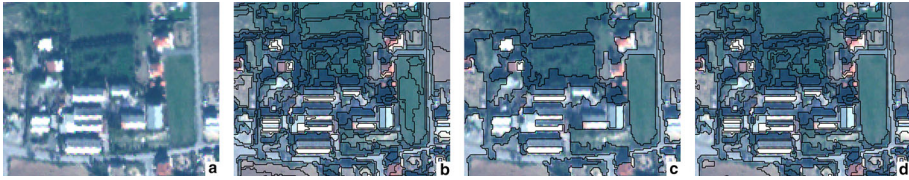


Fig. 4 Multi-level segmentation approach on a subset of the GeoEye-1. **a** input data; image objects at the **b** basic level; **c** final level and **d** optimized level

objects with no significant spectral difference, “Brightness” lower than 10 %, from the super-objects are merged following the shape of the corresponding super-objects in the final level. “Brightness”, here, is the mean value of spectral mean values of all pixels forming an image object; it is calculated by the sum of the mean intensity values of the image layers divided by their quantity calculated for an image object. VIS and NIR bands were used for “Brightness” calculation. Therefore, the optimized level comprises large segments in homogeneous areas and distinctively smaller image objects representing small-scale structures and heterogeneous regions.

The classification procedure was then applied to the image objects at the optimized level. In particular, for each class different spectral and geometric attributes were considered by setting specific thresholds (Fig. 5) based on image interpretation. In the first step, vegetated areas were identified; then, the rules for the outcropping rock, bare soil and water classification were applied on the resulting unclassified objects. Finally, generic impervious surfaces, building (red and other roofs) and roads were classified in order to



Fig. 5 Features and threshold used in the classification rule-set

detect urban areas. Specific rules were applied to avoid misclassification between marl/chalk (outcropping rock) and impervious surfaces due to their similar spectral response (Alexakis et al. 2012). In particular, the image objects belonging to the outcropping rock class were merged; therefore, using shape rules small objects and elongated objects were assigned to impervious surface and roads classes, respectively. Some rules based on contextual features were used to refine the classification results (h in Fig. 3).

3.2.1 Accuracy assessment

The accuracy assessment of the land use/cover map was performed considering 182 targets (Fig. 6). Their selection followed a stratified approach in order to collect approximately the same number of points for each class within the entire area of interest. The reference classes were prior defined by means of photointerpretation, using also the high-resolution natural colour image of the study area available on Google Earth (acquisition 3 December 2011). Moreover, field spectroradiometric campaigns helped to verify the cover class of the check points.

Since the area occupied by water bodies is very limited (0.1 % of the study area), the accuracy of the water class was assessed in a different way. The vector layer of the class was superimposed on the high-resolution image, and the extension was verified by photointerpretation. Therefore, the confusion matrix was computed for the urban areas, vegetation, bare soil and outcropping rock classes.

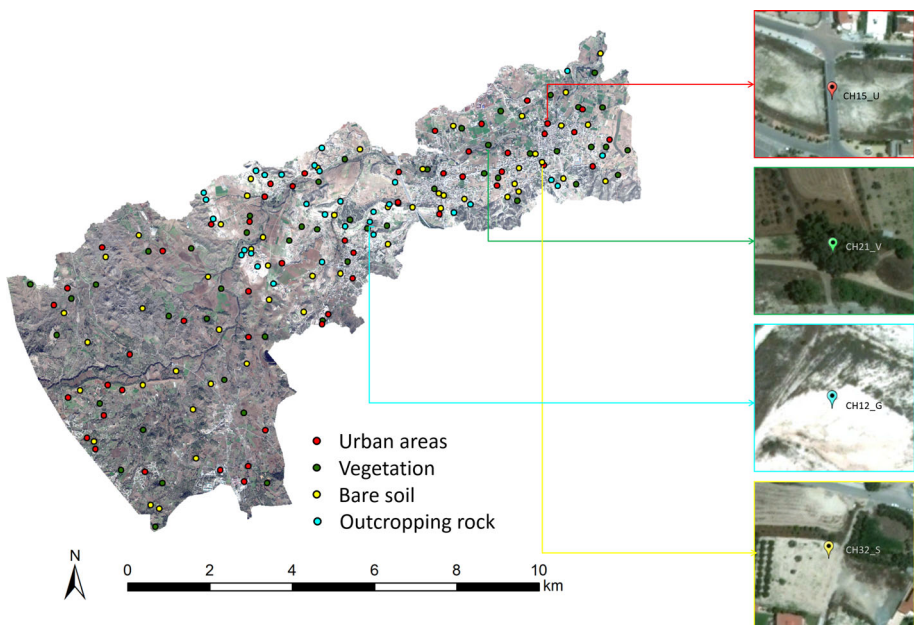


Fig. 6 Ground-truth areas in the GeoEye-1 (*left*) and four examples extracted from high-resolution image of 3-12-2011 (*right*)

3.3 Stream network and morphometric parameters

The stream network of the study area was automatically extracted from the DEM using geoprocessing tools in GIS environment (Magesh et al. 2013) (Fig. 7). The output of this technique produced the stream network and its classification based on Strahler’s system, which designates a segment with no tributaries as a first-order stream, where two first-order stream segments join, they form a second-order stream segment and so on for higher orders (Strahler 1964).

Main linear and areal morphometric parameters, i.e. drainage density (D_d), stream frequency (F_s), elongation ratio (R_e) and form factor (R_f), were computed automatically, according to the studies by Horton (1945), Schumm (1956) and Strahler (1964). D_d indicates the closeness of streams spacing, and it varies with climate and vegetation, soil and rock properties, relief and landscape evolution processes (Shankar and Dharanirajan 2014). D_d values may be 1 km/km² through very permeable rocks, whereas they increase to over 5 km/km² through highly impermeable surfaces (Withanage et al. 2014). Low D_d values generally indicate areas of highly resistant or permeable sub-soil material, dense vegetation and low relief; high D_d is the result of weak or impermeable sub-surface material, sparse vegetation and mountainous relief (Rudraiah et al. 2008). F_s is the total number stream segments of all orders per unit area. A higher stream frequency points to a larger surface run-off and steeper ground surface. The occurrence of stream segments depends on the nature and structure of rocks, vegetation cover, nature and amount of rainfall and soil permeability (Reddy et al. 2004; Magesh et al. 2013). R_e determines the shape of the watershed and generally ranges from values <0.5–1 for more elongated with high relief basins and circular with very low relief basins, respectively (Ramaiah et al. 2012). Regions with low values are susceptible to stronger erosion, whereas regions with high values correspond to high infiltration capacity and low run-off (Parveen et al. 2012). R_f is defined as the ratio of the basin area and square root of the basin length. R_f value would always be <0.754 (for a perfectly circular watershed). Long-narrow basins have larger lengths and therefore smaller R_f . The watershed with high-form factors has high

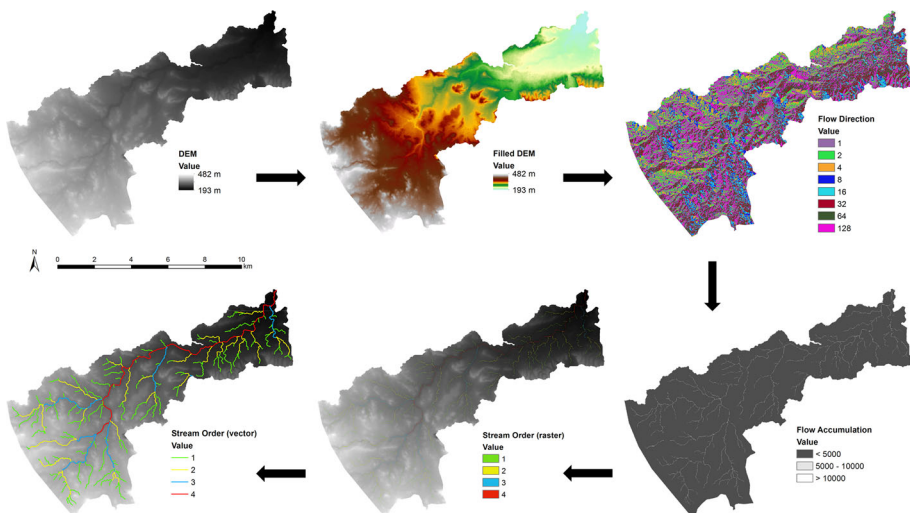


Fig. 7 Workflow for the stream network extraction processing the DEM of the study area

Fig. 8 Five flood-conditioning factors and their reclassification according to the rate of contribution of each to the flood hazard

peak flows of shorter duration, whereas elongated watershed with low-form factor ranges from 0.42 indicating them to be elongated in shape and flow for longer duration (Pareta and Pareta 2011). Table 4 in Sect. 4.2 shows the morphometric parameters computed for the study area.

The stream network was then processed within the bearing, azimuth and drainage (bAd) calculator tool to extract the drainage texture (T) of the study area, one of the factors considered for the generation of the flood hazard map (Dinesh et al. 2012). Following the Smith formula, T was computed as the product of the stream frequency and the drainage density (Smith 1950). T depends upon a number of natural factors such as climate, rainfall, vegetation, rock and soil type, infiltration capacity, relief and stage of development; soft or weak rocks unprotected by vegetation produce a fine texture, whereas massive and resistant rocks cause coarse texture (Sreedevi et al. 2004).

The tool calculates this parameter in a defined grid with a side length of 1 km. In order to generate the T spatial map, the values were interpolated in GIS environment using inverse distance weight (IDW) algorithm. The output cell size was set equal to 5 m (Fig. 8e).

3.4 Multi-criteria analysis

A multi-criteria analysis (MCA) was performed to compute the flood hazard index (FHI) considering the five flood-conditioning factors: slope, distance to main channels, drainage texture, geology and land use/cover. In particular, a GIS-based AHP (analytic hierarchy process) approach was used for comparing each factor map and determining the factor weight values. The FHI was then computed using a weighted overlay analysis and the raster calculator in GIS environment:

$$\text{FHI} = \sum w_i * x_i \quad (1)$$

where w_i = weight of factor i and x_i = score of factor i .

3.4.1 Factor ranking assignation

Since criteria were measured on different scales, the factor maps were reclassified in order to be correlated with the flood hazard. Generally, the numerical ranking of every factor is performed by experts on the basis of the available information about the area and their experience. Here, different classes were defined for each factor, following common practices described in the literature; then, the rank values listed in Table 2 were assigned. The idea is trying to quantify the rate of contribution of each factor to the flood hazard.

Slope is an important factor to identify zones that have shown high susceptibility to flooding over the years due to low slope gradient (Fernández and Lutz 2010). The slope influences the direction and the amount of surface run-off reaching a site. Rainfall or excess of water from a river gathers in correspondence of areas characterized by low slope values; thus, flat areas are highly subjected to water logging and flood occurrences compared to steep zones, which are more exposed to surface run-off (Ouma and Tateishi 2014). The slope map was prepared in GIS environment in per cent grade, using the 5-m pixel DEM of the study area; the values were subdivided into four classes as listed in Table 2.

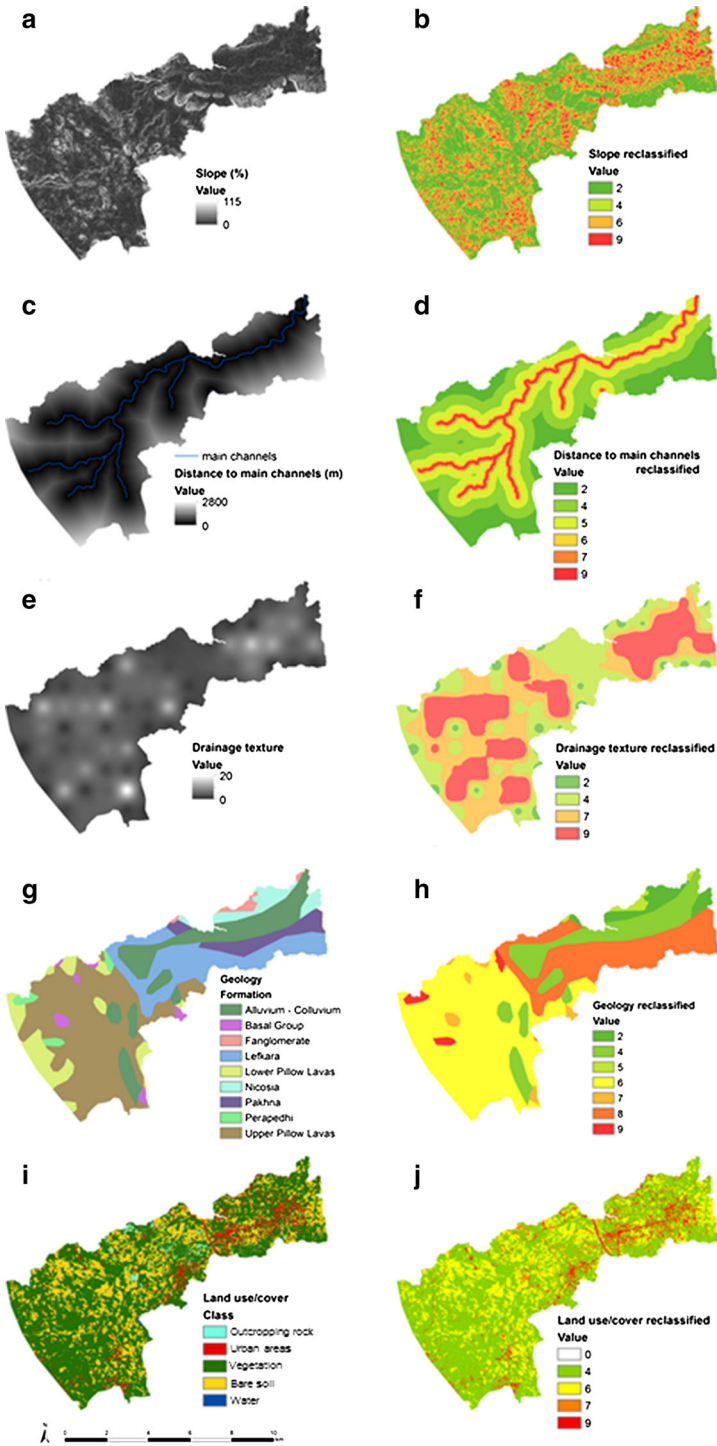


Table 2 Rank value for each factor

Factor	Classes	Rank
Slope (%)	<2	9
	2–5	6
	5–8	4
	>8	2
Distance to main channels (m)	<50	9
	50–100	7
	100–200	6
	200–500	5
	500–1000	4
Drainage texture	>1000	2
	<4	2
	4–10	4
	10–15	7
Geology	>15	9
	Schists	9
	Marls, chalks	8
	Igneous rock	7
	Volcanic rocks	6
	Fanglomerate	5
	Alluvium	4
Land use/cover	Limestones	3
	Sandstones	2
	Urban areas	9
	Outcropping rock	7
	Bare soil	6
	Vegetation	4

According to the records of the Department of Water Development of Cyprus, the most affected areas during flooding event in Yialias river are those near the main channel as a consequence of water overflow. The main channels were extracted from the stream network layer among streams of 3th and 4th orders. Thus, all the areas from both sides of the channels were mapped in GIS environment calculating the Euclidean distance. Rank value was assigned to each zone in relation to its proximity to the channels (Table 2).

Drainage texture (also defined Infiltration number) is an important parameter in observing the infiltration characteristic of the basin. It is inversely proportional to the infiltration capacity; therefore, high values indicate a very low infiltration capacity, resulting in high run-off triggering flooding (Hajam et al. 2013; Shankar and Dharanirajan 2014). Based on Smith classification (Smith 1950), drainage texture map was subdivided into four class and reclassified assigning the rank values (Table 2).

In the geological map of the study area, major geological formations were considered and ranked depending to their rate of hydraulic conductivity (Civita 2005) (Table 2).

Rainwater run-off is much more likely on bare fields than those with a good crop cover. The presence of thick vegetative cover reduces the amount of run-off. On the other hand, impermeable surfaces such as concrete absorb almost no water at all. Impervious surfaces

such as buildings, roads and generally urban constructions decrease the soil infiltration capacity increasing the run-off. Urbanization typically leads to the decrease in lag time and the increase in the peak discharge (Weng 2001; Krishnamurthy and Jayaprakash 2013; Ouma and Tateishi 2014). In compliance of these considerations, the land use/cover map of the study area was resampled to 5-m pixel size considering modal values and then reclassified (Table 2).

3.4.2 Factor weights evaluation: AHP application

After the rank values assignment, the AHP method was used for extracting the weight of each factor in order to consider its relative importance in the FHI computation.

In developing weights, the pairwise comparison matrix was compiled evaluating every possible pairing. The relative importance between two criteria involved in determining the stated objective was quantified using a nine-point continuous scale (Saaty 1980; Ouma and Tateishi 2014). Pairwise judgments were based on the information available and the author knowledge and experience.

The weight of each criterion can be derived by taking the principal eigenvector of the square reciprocal matrix of pairwise comparisons between the criteria. A good approximation to this result was achieved by summing the values in each column of the pairwise comparison matrix; dividing each element in the matrix by its column total (normalized pairwise comparison matrix); and finally computing the average of the elements in each row of the normalized matrix (Drobne and Liseč 2009) (Table 5).

To determine the degree of consistency that was used in developing the ratings, consistency ratio (CR) was calculated. CR defines the probability that the matrix ratings were randomly generated, and Saaty (1980) suggests that matrices with CR ratings greater than 0.10 should be re-evaluated. It is defined as:

$$CR = CI/RI \quad (2)$$

Random index (RI) is the consistency index of the randomly generated pairwise comparison matrix, which depends on the number of elements compared. In this case, RI is equal to 1.12 (Ouma and Tateishi 2014). Consistency index (CI) provides a measure of departure from consistency:

$$CI = (\lambda - n)/(n - 1) \quad (3)$$

where λ is the average value of the consistency vector and n is the number of criteria. The estimation of the CR involved: the determination of the weighted sum vector by multiplying the weight for the first criterion times the first column of the original pairwise comparison matrix, then multiplying the second weight times the second column of the original pairwise matrix, and so on to the fifth weight; the sum of these values over the rows; the determination of the consistency vector by dividing the weighted sum vector by the criterion weights previously determined.

3.5 Flood hazard map

The FHI was classified into qualitative categories for a visual and easy interpretation of the hazard scenario. The natural breaks method was used to determine the number of hazard classes and break points between classes depending on the natural patterns in which the

data are clustered. This technique attempts to reduce the variance within classes and maximize the variance between classes (Stefanidis and Stathis 2013; Asare-Kyei et al. 2015). In particular, the FHI cumulative frequency curve, along with its first derivative, was computed for identifying the break points and setting class boundaries where the slope substantially changes (Cervi et al. 2010) (Fig. 9).

4 Results

4.1 Land use/cover map

The land use/cover map of the study area, resulted from the object-based classification of the GeoEye-1, is shown in Fig. 8i. Almost the 67 % (46.83 km²) of the study area is covered by vegetation; the bare soil occupies 17.95 km² (about to 26 % of the whole area) and the remaining 7 % is covered by urban areas (4.22 km²), outcropping rock (1.03 km²) and water (0.04 km²) classes.

The accuracy assessment results are presented in Table 3. For urban areas, vegetation, bare soil and outcropping rock classes, an overall accuracy equal to the 89.5 % was achieved. Relevant errors are attributable to the commission of the outcropping rock class. Some urban areas, in particular portions of roads or impervious surfaces, remain in the outcropping rock class even after applying the geometric rules to avoid this misclassification. Moreover, probably due to the presence of aggregates containing marl/chalk, some image objects belonging to bare soil were assigned to the outcropping rock class.

4.2 Stream network and morphometric parameters

The stream network classification, based on Strahler's system and performed in GIS environment, revealed that the drainage network is of fourth order.

Linear and areal morphometric parameters computed for the study area are listed in Table 4. In particular, a D_d value equal to 2.19 km/km² was obtained. According to the Strahler's classification, the study area is characterized by low drainage density (<5)

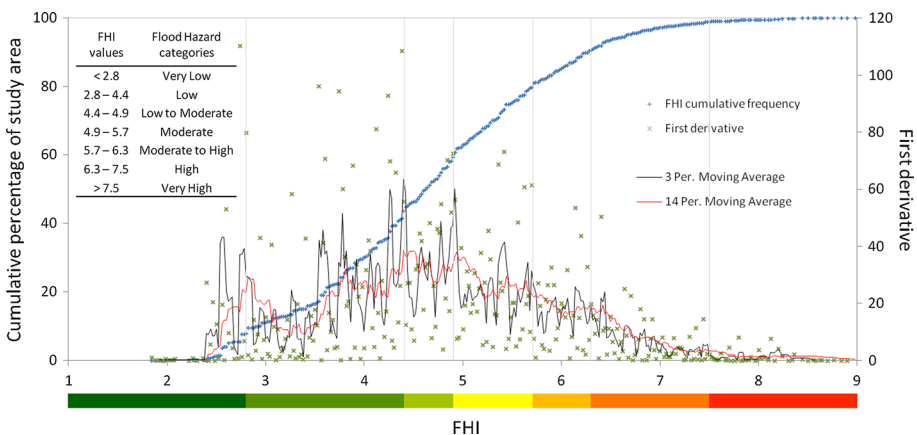


fig. 9 FHI cumulative frequency diagram

Table 3 Confusion matrix for the land use/cover map

11 December 2011		Ground truth (pixels)			
Class	Urban areas	Vegetation	Bare soil	Outcropping rock	Total
Urban areas	43	0	1	0	44
Vegetation	0	47	3	0	50
Bare soil	1	3	43	0	47
Outcropping rock	6	0	5	30	41
Total	50	50	52	30	182
Overall accuracy	(163/182)	89.56 %			
Kappa coefficient	0.860				

Class	Commission (%)	Omission (%)	User Acc. (%)	Proc. Acc. (%)
Urban areas	2.3	14.0	97.7	86.0
Vegetation	6.0	6.0	94.0	94.0
Bare soil	8.5	17.3	91.5	82.7
Outcropping rock	26.8	0.0	73.2	100.0

Table 4 Some linear and areal morphometric parameters of the study area

Parameter	Formula	Value	Reference	Description
Perimeter (km)	P	75.32		
Area (km ²)	A	70.11		
Stream total number	N_u	185.00	Strahler (1964)	
Stream total length (km)	L_u	153.20	Horton (1945)	
Basin length (km)	L_b	15.20	Schumm (1956)	
Drainage density (km/km ²)	$D_d = L_u/A$	2.19	Horton (1945)	Closeness of streams spacing ~1 km/km ² highly permeable rocks >5 km/km ² impermeable surfaces
Stream frequency (km ⁻²)	$F_s = N_u/A$	2.64	Horton (1945)	Stream segments per unit area <1 km ⁻² high permeable geology and low relief >5 km ⁻² impermeable sub-surface material and steep surface
Elongation ratio	$R_e = 2*(A/\pi)^{1/2}/L_b$	0.62	Schumm (1956)	Determines the shape of the watershed circular (0.9–1), oval (0.8–0.9), less elongated (0.7–0.8), elongated (0.5–0.7), more elongated (<0.5)
Form factor	$R_f = A/L_b^2$	0.30	Horton (1945)	0.7854 for a perfectly circular basin, smaller the value, more elongated will be the basin

suggesting permeable rock formations, low relief and dense vegetation. This consideration is further confirmed by a low F_s value.

For the study area, the R_e is equal to 0.62, indicating that the basin is elongated with relatively moderate relief and erosion. The low R_f equal to 0.30 confirms the elongated shape of the region.

4.3 Multi-criteria analysis

The thematic maps of the five flood-conditioning factors, prepared in GIS environment by assigning rank values for each class of each factor, are presented in Fig. 8.

In order to assess their influence on flooding, the pairwise comparison matrix was compiled, using the nine-point scale suggested by Saaty (Saaty 1980) (Table 5). The derived relative weight of each factor and the CR value is listed in Table 5. A CR equal to 0.055 (smaller than 0.1) was achieved, proving the pairwise matrix consistency and the factor weights reliability.

The FHI was then computed in GIS environment in the form of digital map. Figure 10a shows the FHI map produced by using the weighted linear combination (Eq. 1):

$$\text{FHI} = 0.260 * \text{Slope} + 0.503 * \text{Distance to main channels} + 0.068 * \text{Drainage texture} + 0.035 * \text{Geology} + 0.134 * \text{Land use/cover} \quad (4)$$

FHI values were found to range between 1.83 and 8.96. The higher pixel values of FHI are the most susceptible to floods; conversely, the lower values are the least susceptible.

4.4 Flood hazard map

The flood hazard zoning map was produced classifying the FHI map into different qualitative categories. In particular, seven hazard categories ranging from very low to very high were identified using the natural breaks method (see Sect. 3.5). Figure 9 shows the FHI cumulative frequency curve that allowed to select the break point values. Finally, in (Fig. 10b) the flood hazard map is presented.

Clearly, the most dangerous zones are flat areas located close to main channels, while high slope gradients areas, in general covered by vegetation, are less sensitive to floods. Figure 11a shows the summary statistics computed for each hazard class, in terms of percentage of the whole area under investigation. Almost the 60 % of the study area was classified between “very low” and “moderate to low” flood hazard categories; the “moderate” hazard lands cover about the 20 % and lands between “moderate to high” to “very high” flood hazard classes represent the 20 %.

Information about flood hazard relating to land use/cover type, obtained by GIS zonal overlay, is presented in Fig. 11b. “Very high” class covers the 1 % of the whole area, mainly composed by vegetated areas and bare soil. Urban areas are largely comprised in

Table 5 Application of AHP approach: pairwise matrix, consistency indicators and factor weights

	Slope	Distance to mail channels	Drainage texture	Geology	Land use/cover	weight
Slope	1	1/3	5	7	3	0.260
Distance to main channels	3	1	7	9	5	0.503
Drainage texture	1/5	1/7	1	3	1/3	0.068
Geology	1/7	1/9	1/3	1	1/5	0.035
Land use/cover	1/3	1/5	3	5	1	0.134
AHP indicators	$\lambda = 5.248$	CI = 0.062	CR = 0.055			

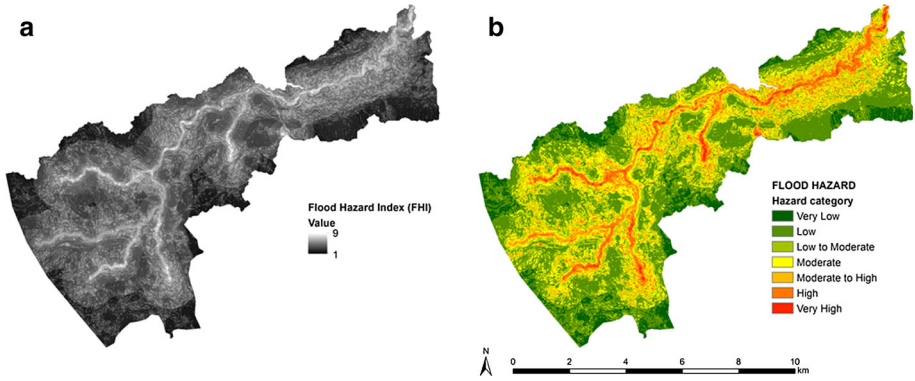


Fig. 10 a The FHI digital map and b the flood hazard zoning map

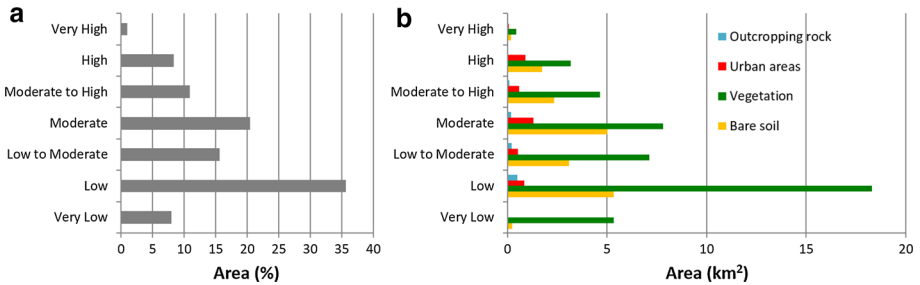


Fig. 11 a Percentage of the study area belonging to each hazard category and b land use/cover type (km²) for each flood hazard category

the “moderate” category (1.31 km²), but a significant part, equal to the 21 % of the whole urban class (0.89 km²), is ranked as “high” flood hazard zone.

The situation appears alarming along the whole length of the river, with particular reference to some sections at Pera Chorio and Dali villages where extensive anthropogenic interventions can be observed in correspondence of the riverbed (Fig. 12). In these zones, the results have been confirmed by the visual comparison with the flood extent map produced by the WDD (Water Development Department 2014a) (Fig. 12b). These flood extent maps are in line with the Directive 2007/60 of the European Commission, which is compulsory for all member states. The maps were based on historical data and/or other available data, in order to identify areas of potentially serious floods risks. These risk maps were produced for three different flood scenarios: (a) flood with probability 1 in 500 years (low probability that rare/extreme event); (b) flood with probability 1 in 100 years (average probability); and (c) flood with probability 1–20 years (high probability). For each of the above-mentioned scenario, both the flood extent and the depth of water were estimated. Moreover, other parameters such as the indicative number of inhabitants potentially affected; the type of the economic/cultural/archaeological significance activity of the area potentially affected; installations that might cause accidental pollution in case of flooding and other potential pollution sources have been also considered. Based on the legislation of Cyprus, the above-mentioned maps should be updated every 6 years.

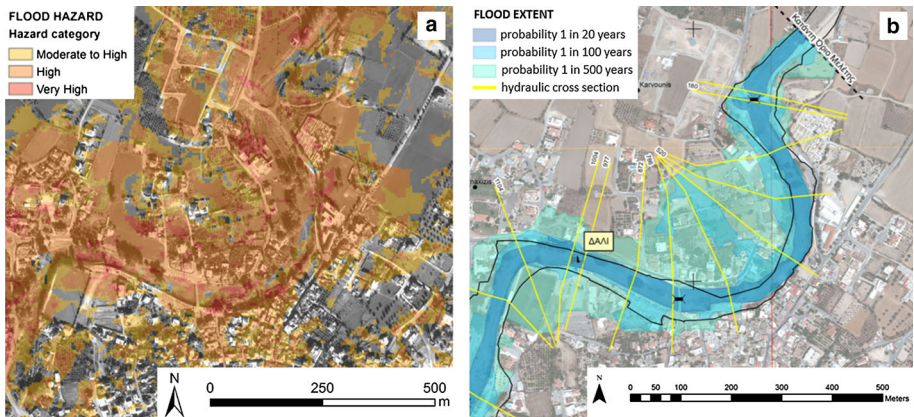


Fig. 12 Dali village: **a** flood hazard categories superimposed to GeoEye-1 satellite image; **b** flood extent map produced by the WDD (Water Development Department 2014b)

5 Conclusions

A multi-criteria analysis (MCA) assisted by GIS was performed to produce an easily readable and rapidly accessible flood hazard map for an area where a quantitative method based on numerical modelling is not feasible, because of the lack of some essential data. The presented approach was tested on the Yialias river basin. Only the riskiest portion was considered, but this limitation did not affect the hazard analysis. Five flood-conditioning factors—i.e. slope, distance to main channels, drainage texture, geology and land use/cover—were considered by means of weighted linear combination to compute the flood hazard index (FHI). The analytic hierarchy process (AHP) approach was used for deriving the relative importance, the weight, of each criterion. Once achieved the weights, FHI was computed and presented in the form of flood hazard zoning map. FHI value ranges were associated with seven hazard categories by means of the natural breaks technique.

The MCA/AHP approach was found to be useful for flood hazard assessment of the study area thanks to its capability in handling scarcity of data and its effectiveness in analysing large areas. In fact, it is noteworthy that, apart from the geological map, all the information was derived from satellite remote sensing.

The land use/cover map of the study area was obtained performing object-based supervised classification on the GeoEye-1 satellite image. The modular structure developed for this procedure may be easily applied to other images, because the user can rapidly adjust segmentation parameters and rule thresholds depending on the input data.

FHI was computed integrating land use/cover map, geological data and morphological factors, derived from 5-m resolution DEM. Clearly, the computation can be improved as long as more information, such as longer rainfall/flood records, is available. Further improvement can be achieved by refining the AHP approach, working iteratively with the experts.

The hazard zoning map can allow to deepen the knowledge about flood risk in the study area, and it can be used as a first-stage analysis for identifying most vulnerable areas, to take decision in sustainable land management perspective and to formulate mitigation strategy. Moreover, specific surveys can be planned to perform more accurate analysis in correspondence of high flood hazard areas.

From the study results, it was observed that MCA/AHP along with GIS offers a flexible, step-by-step and transparent way for analysing complex problems. The applied technique can be easily extended to other areas; in fact, according to the characteristics and the available data of the study area, additional factors can be defined and the relative weights for all factors can be re-estimated. Clearly, this extension is not automatic, because the thresholds in the classification, the selection of the factors and the tuning of the ranking are to be accommodated by experts according to the local peculiarities. The whole processing chain, however, can be reproduced in other areas maintaining the same structure thanks to its inner flexibility and the fact that it relies mainly on remote sensing data available worldwide.

References

- Alexakis DD, Hadjimitsis DG, Agapiou A et al (2012) Monitoring urban land cover using satellite remote sensing techniques and field spectroradiometric measurements: case study of “Yialias” catchment area in Cyprus. *J Appl Remote Sens* 6:1–14. doi:[10.1117/1.JRS.6.063603](https://doi.org/10.1117/1.JRS.6.063603)
- Alexakis DD, Hadjimitsis DG, Agapiou A (2013) Estimating flash flood discharge in a catchment area with the use of hydraulic model and terrestrial laser scanner. In: Helmis CG, Nastos PT (eds) *Advances in meteorology, climatology and atmospheric physics*. Springer, Heidelberg, pp 9–15
- Altan O, Backhaus R, Boccardo P et al (2013) The value of geoinformation for disaster and risk management (VALID) benefit analysis and stakeholder assessment. Joint Board of Geospatial Information Societies, Copenhagen
- Asare-Kyei D, Forkuor G, Venus V (2015) Modeling flood hazard zones at the sub-district level with the rational model integrated with GIS and remote sensing approaches. *Water* 7:3531–3564. doi:[10.3390/w7073531](https://doi.org/10.3390/w7073531)
- Baatz M, Schäpe A (2000) Multiresolution segmentation: an optimization approach for high quality multi-scale image segmentation. In: Strobl J, Blaschke T, Griesebner G (eds) *Angewandte geographische informationsverarbeitung XII AGIT symposium*. Salzburg, Germany, pp 12–23
- Benz UC, Hofmann P, Willhauck G et al (2004) Multi-resolution, object-oriented fuzzy analysis of remote sensing data for GIS-ready information. *ISPRS J Photogramm Remote Sens* 58:239–258. doi:[10.1016/j.isprsjprs.2003.10.002](https://doi.org/10.1016/j.isprsjprs.2003.10.002)
- Bhaskaran S, Paramananda S, Ramnarayan M (2010) Per-pixel and object-oriented classification methods for mapping urban features using Ikonos satellite data. *Appl Geogr* 30:650–665. doi:[10.1016/j.apgeog.2010.01.009](https://doi.org/10.1016/j.apgeog.2010.01.009)
- Bitelli G, Camassi R, Gusella L, Mogno A (2004) Image change detection on urban area: the earthquake case. *Int Arch Photogramm Remote Sens Spat Inf Sci XXXV*:692–697
- Boccardo P (2013) New perspectives in emergency mapping. *Eur J Remote Sens* 46:571–582. doi:[10.5721/EuJRS20134633](https://doi.org/10.5721/EuJRS20134633)
- Brivio PA, Colombo R, Maggi M, Tomasoni R (2002) Integration of remote sensing data and GIS for accurate mapping of flooded areas. *Int J Remote Sens* 23:429–441. doi:[10.1080/01431160010014729](https://doi.org/10.1080/01431160010014729)
- Bruzzone L, Carlin L (2006) A multilevel context-based system for classification of very high spatial resolution images. *IEEE Trans Geosci Remote Sens* 44:2587–2600. doi:[10.1109/TGRS.2006.875360](https://doi.org/10.1109/TGRS.2006.875360)
- Büchele B, Kreibich H, Kron A et al (2006) Flood-risk mapping: contributions towards an enhanced assessment of extreme events and associated risks. *Nat Hazards Earth Syst Sci* 6:485–503. doi:[10.5194/nhess-6-485-2006](https://doi.org/10.5194/nhess-6-485-2006)
- Carver SJ (1991) Integrating multi-criteria evaluation with geographical information systems. *Int J Geogr Inf Syst* 5:321–339. doi:[10.1080/02693799108927858](https://doi.org/10.1080/02693799108927858)
- Cervi F (2009) Weight of evidence and artificial neural networks for potential groundwater spring mapping: an application to the Mt. Modino area (Northern Apennines, Italy). *Geomorphology* 111:79–87. doi:[10.1016/j.geomorph.2008.03.015](https://doi.org/10.1016/j.geomorph.2008.03.015)
- Cervi F, Berti M, Borgatti L et al (2010) Comparing predictive capability of statistical and deterministic methods for landslide susceptibility mapping: a case study in the northern Apennines (Reggio Emilia Province, Italy). *Landslides* 7:433–444. doi:[10.1007/s10346-010-0207-y](https://doi.org/10.1007/s10346-010-0207-y)

- Chen Y, Barrett D, Liu R et al (2014) A spatial framework for regional-scale flooding risk assessment. In: Ames DP, Quinn NWT, Rizzoli AE (eds) 7th International congress on environmental modelling and software modelling. San Diego, USA
- Civita M (2005) *Idrogeologia applicata e ambientale*, CEA-Casa Editrice Ambrosiana
- Dewan A (2013) Hazards, risk and vulnerability. In: *Floods in a megacity: geospatial techniques in assessing hazards, risk and vulnerability*. Springer, Netherlands, Dordrecht, pp 35–74. doi:[10.1007/978-94-007-5875-9_2](https://doi.org/10.1007/978-94-007-5875-9_2)
- Dinesh AC, Joseph Markose V, Jayappa KS (2012) Bearing, azimuth and drainage (bAd) calculator: a new GIS supported tool for quantitative analyses of drainage networks and watershed parameters. *Comput Geosci* 48:67–72. doi:[10.1016/j.cageo.2012.05.016](https://doi.org/10.1016/j.cageo.2012.05.016)
- Drobne S, Lisec A (2009) Multi-attribute decision analysis in GIS: weighted linear combination and ordered weighted averaging. *Informatica* 33:459–474
- Fernández DS, Lutz MA (2010) Urban flood hazard zoning in Tucumán Province, Argentina, using GIS and multicriteria decision analysis. *Eng Geol* 111:90–98. doi:[10.1016/j.enggeo.2009.12.006](https://doi.org/10.1016/j.enggeo.2009.12.006)
- Franci F, Lambertini A, Bitelli G (2014) Integration of different geospatial data in urban areas: a case of study. In: Hadjimitsis DG, Themistocleous K, Michaelides S, Papadavid G (eds) *Proceedings of SPIE*. pp 92290P1–9. doi:[10.1117/12.2066614](https://doi.org/10.1117/12.2066614)
- Franci F, Mandanici E, Bitelli G (2015) Remote sensing analysis for flood risk management in urban sprawl contexts. *Geomat Nat Hazards Risk* 6:583–599. doi:[10.1080/19475705.2014.913695](https://doi.org/10.1080/19475705.2014.913695)
- Garschagen M, Mucke P, Schaubert A et al (2014) *WorldRiskReport 2014*. Bündnis Entwicklung Hilft (Alliance Development Works) and United Nations University–Institute for Environment and Human Security (UNU-EHS)
- Gianinetto M, Villa P, Lechi G (2006) Postflood damage evaluation using landsat TM and ETM+ data integrated with DEM. *IEEE Trans Geosci Remote Sens* 44:236–243. doi:[10.1109/TGRS.2005.859952](https://doi.org/10.1109/TGRS.2005.859952)
- Gusella L, Adams BJ, Bitelli G (2007) Use of mobile mapping technology for post-disaster damage information collection and integration with remote sensing imagery. In: *Proceedings of 5th international symposium on mobile mapping technology*
- Hajam RA, Aadil H, SamiUllah B (2013) Application of morphometric analysis for geo-hydrological studies using geo-spatial technology—a case study of Vishav drainage basin. *J Waste Water Treat Anal* 04:1–12. doi:[10.4172/2157-7587.1000157](https://doi.org/10.4172/2157-7587.1000157)
- Horton RE (1945) Erosional development of streams and their drainage basins; hydrophysical approach to quantitative morphology. *Geol Soc Am Bull* 56:275–370
- Kandilioti G, Makropoulos C (2011) Preliminary flood risk assessment: the case of Athens. *Nat Hazards* 61:441–468. doi:[10.1007/s11069-011-9930-5](https://doi.org/10.1007/s11069-011-9930-5)
- Krishnamurthy R, Jayaprakash M (2013) Flood hazard assessment of vamanapuram river basin, Kerala, India: an approach using remote sensing and GIS techniques. *Adv Appl Sci Res* 4:263–274
- Kron W (2005) Flood risk=hazard values vulnerability. *Water Int* 30:58–68. doi:[10.1080/02508060508691837](https://doi.org/10.1080/02508060508691837)
- Lawal D, Matori A (2012) Detecting flood susceptible areas using GIS-based analytic hierarchy process. *Int Conf Future Environ Energy IPCBEE* 28:4–8
- Magesh NS, Jitheshlal KV, Chandrasekar N, Jini KV (2013) Geographical information system-based morphometric analysis of Bharathapuzha river basin, Kerala, India. *Appl Water Sci* 3:467–477. doi:[10.1007/s13201-013-0095-0](https://doi.org/10.1007/s13201-013-0095-0)
- Malczewski J (2006) GIS-based multicriteria decision analysis: a survey of the literature. *Int J Geogr Inf Sci* 20:703–726. doi:[10.1080/13658810600661508](https://doi.org/10.1080/13658810600661508)
- Munich RE (2014) *NatCatSERVICE loss events worldwide 1980–2013*. München, Germany
- Musungu K, Motala S, Smit J (2012) Using multi-criteria evaluation and GIS for flood risk analysis in informal settlements of cape town: the case of Graveyard Pond. *S Afr J Geomat* 1:77–91
- Ouma Y, Tateishi R (2014) Urban flood vulnerability and risk mapping using integrated multi-parametric AHP and GIS: methodological overview and case study assessment. *Water* 6:1515–1545. doi:[10.3390/w6061515](https://doi.org/10.3390/w6061515)
- Pareta K, Pareta U (2011) Quantitative morphometric analysis of a watershed of Yamuna basin, India using ASTER (DEM) data and GIS. *Int J Geomatics Geosci* 2:248–269
- Parveen R, Kumar U, Singh VK (2012) Geomorphometric characterization of upper South Koel basin, Jharkhand: a remote sensing and GIS approach. *J Water Resour Prot* 4:1042–1050
- Pavlis NK, Holmes SA, Kenyon SC, Factor JK (2012) The development and evaluation of the earth gravitational model 2008 (EGM2008). *J Geophys Res* 117:B04406. doi:[10.1029/2011JB008916](https://doi.org/10.1029/2011JB008916)
- Pradhan B (2010) Flood susceptible mapping and risk area delineation using logistic regression, GIS and remote sensing. *J Spat Hydrol* 9(2)

- Rahmati O, Zeinivand H, Besharat M (2015) Flood hazard zoning in Yasooj region, Iran, using GIS and multi-criteria decision analysis. *Geomat Nat Hazards Risk* 5705:1–18. doi:10.1080/19475705.2015.1045043
- Ramaiah SN, Gopalakrishna GS, Vittala SS, Najeeb K (2012) Morphometric analysis of sub-basins in and around Malur Taluk, Kolar district, Karnataka using remote sensing and GIS techniques. *Nat Environ Pollut Technol* 11:89–94
- Reddy GPO, Maji AK, Gajbhiye KS (2004) Drainage morphometry and its influence on landform characteristics in a basaltic terrain, Central India—a remote sensing and GIS approach. *Int J Appl Earth Obs Geoinf* 6:1–16. doi:10.1016/j.jag.2004.06.003
- Rudraiah M, Govindaiah S, Vittala S (2008) Morphometry using remote sensing and GIS techniques in the sub-basins of Kagna river basin, Gulburga district, Karnataka, India. *J Indian Soc Remote Sens* 36:351–360
- Saaty TL (1980) *The analytic hierarchy process: planning, priority setting, resources allocation*. McGraw, New York
- Schiewe J (2002) Segmentation of high-resolution remotely sensed data—concepts, applications and problems. *Int Arch Photogramm Remote Sens Spat Inf Sci* 34:380–385
- Schumm SA (1956) *Evolution of drainage system and slopes in badlands of Perth Amboy, New Jersey*. *Geol Soc Am Bull* 67:597–646
- Shankar S, Dharanirajan K (2014) Drainage morphometry of flood prone rangat watershed, middle Andaman, India—a geospatial approach. *Int J Innov Technol Explor Eng* 3:15–22
- Siddayao GP, Valdez SE, Fernandez PL (2014) Analytic hierarchy process (AHP) in spatial modeling for floodplain risk assessment. *Int J Mach Learn Comput* 4:450–457. doi:10.7763/IJMLC.2014.V4.453
- Sinha R, Bapalu GV, Singh LK, Rath B (2008) Flood risk analysis in the Kosi river basin, North Bihar using multi-parametric approach of analytical hierarchy process (AHP). *J Indian Soc Remote Sens* 36:293–307
- Smith KG (1950) Standards for grading texture of erosional topography. *Am J Sci* 248:655–668. doi:10.2475/ajs.248.9.655
- Sreedevi PD, Subrahmanyam K, Ahmed S (2004) The significance of morphometric analysis for obtaining groundwater potential zones in a structurally controlled terrain. *Environ Geol* 47:412–420. doi:10.1007/s00254-004-1166-1
- Stefanidis S, Stathis D (2013) Assessment of flood hazard based on natural and anthropogenic factors using analytic hierarchy process (AHP). *Nat Hazards* 68:569–585. doi:10.1007/s11069-013-0639-5
- Strahler AN (1964) Quantitative geomorphology of drainage basins and channel networks. In: Chow VT (ed) *Handbook of applied hydrology*. McGraw Hill Book Company, New York, pp 4–35
- Taubenböck H, Esch T, Wurm M et al (2010) Object-based feature extraction using high spatial resolution satellite data of urban areas. *J Spat Sci* 55:117–132. doi:10.1080/14498596.2010.487854
- United Nations Inter-Agency Secretariat of the International Strategy for Disaster Reduction UN/ISDR (2004) *Living with risk: a global review of disaster reduction initiatives*. United Nations, New York
- Van Westen CJ (2013) Remote sensing and GIS for natural hazards assessment and disaster risk management. In: Shroder J, Bishop MP (eds) *Treatise on geomorphology*. Elsevier, San Diego, pp 259–298
- Wang Y, Li Z, Tang Z, Zeng G (2011) A GIS-based spatial multi-criteria approach for flood risk assessment in the Dongting Lake Region, Hunan, Central China. *Water Resour Manag* 25:3465–3484. doi:10.1007/s11269-011-9866-2
- Water Development Department R of C (2014a) Flood hazard maps and flood risk maps—2014. <http://www.cyprus.gov.cy/moa/wdd/wdd.nsf/all/410903B9E6BB3FF5C2257D2D003B0D46?opendocument>. Accessed 28 Nov 2015
- Water Development Department R of C (2014b) Flood hazard maps and flood risk maps—2014
- Weng Q (2001) Modeling urban growth effects on surface runoff with the integration of remote sensing and gis. *Environ Manag* 28:737–748. doi:10.1007/s002670010258
- Withanage NS, Dayawansa NDK, De Silva RP (2014) Morphometric analysis of the Gal Oya river basin using spatial data derived from GIS. *Trop Agric Res* 26:175–188
- Yahaya S, Ahmad N, Abdalla RF (2010) Multicriteria analysis for flood vulnerable areas in Hadejia-Jama'are river Basin, Nigeria. *Eur J Sci Res* 42:71–83